



Integrated satellite imagery and electrical resistivity analysis of underground mine-induced subsidence and associated risk assessment of Barapukuria coal mine, Bangladesh

Md. Imam Sohel Hossain¹ · Md. Sha Alam¹ · Pradip Kumar Biswas¹ · Md. Shohel Rana¹ · Mst. Shanjida Sultana¹ · Mohammad Nazim Zaman¹ · Md Abdus Samad³ · Md Jamilur Rahman² · A. S. M. Woobaiddullah²

Received: 8 May 2023 / Accepted: 23 September 2023

© The Author(s), under exclusive licence to Springer-Verlag GmbH Germany, part of Springer Nature 2023

Abstract

This study addresses the critical issue of land subsidence in densely populated agriculture-based country, Bangladesh, focusing on the Barapukuria coal mine area. Our research employed time-series analysis of Landsat satellite imagery from 2005 to 2020, coupled with vertical electrical sounding resistivity methods. Through the false color composite image analysis in Earth Engine and GIS-based mapping, we quantified the areal extent of subsidence, and results were validated by field visits and cross-referencing with ESRI and dynamic world land use–land cover maps. Our study revealed a concerning trend of subsidence moving from west to east, towards the two nearby residential areas. Most importantly, the rate of areal extent of subsidence was alarming (17.4 acres per year), resulting in a cumulative loss of 205 acres since 2008. Linear regression predicts that this subsided area will double to around 405 acres by 2030, indicating significant risk to nearby communities. The trajectory of subsidence extent led us to examine the subsurface condition of nearby villages using calibrated vertical electrical sounding and borehole data. This revealed a higher resistivity in the northern area, indicating a future subsidence risk compared to the southern part. This was further confirmed by subsurface lithology, composed mainly of Holocene deposits containing clay, clayey sand, and sand. These layers, with their inherent instability and higher consolidation potential, exhibited higher resistivity and more prone to land subsidence. Overall, this study provides valuable insights for predicting subsidence, assessing associated risks, and guiding policy decisions to prevent future damage and facilitate community rehabilitation.

Keywords Barapukuria coal mine · Land subsidence · Satellite time series image analysis · Change detection · Resistivity method

Introduction

Land subsidence induced by underground coal mining has been a major concern for many countries around the world (Del Conte and Falorni 2019; Bagheri et al. 2021; Dang

et al. 2021). The consequences of such subsidence can range from minor infrastructure damage to catastrophic environmental and social impacts. These effects can have significant impacts on the environment and the local economy. That said, there is a growing concern of geo-hazards due to coal mining as a critical construct in environmental science in general and its impacts in particular. As a result, substantial research interest has been generated in the area of geo-hazards due to mining activities around the world (Pacheco-Martínez et al. 2015; Del Conte and Falorni 2019; Abubakar et al. 2020; Oliver-Cabrera et al. 2020; Widada et al. 2020; Abubakar and Shanmugaveloo 2021; Dang et al. 2021).

The Barapukuria coal mine in Bangladesh stands as a prominent contributor to the national economy, generating significant revenue annually (BCMCL 2023). Despite its economic benefits, the mine also poses environmental

✉ Md. Imam Sohel Hossain
imam_immm@bcsir.gov.bd

¹ Institute of Mining, Mineralogy and Metallurgy (IMMM), Bangladesh Council of Scientific and Industrial Research (BCSIR), Khanjonpur, Joypurhat 5900, Bangladesh

² Department of Geology, University of Dhaka, Dhaka 1000, Bangladesh

³ National Centre for Physical Acoustics and Department of Civil Engineering, University of Mississippi, University, MS 38677, USA

challenges, particularly in the form of land subsidence (Alam et al. 2022; Arifeen et al. 2021; Islam and Chakraborty 2021; Howladar 2016a). The subsidence issue is a major concern due to the high population density (~ 1125 people per square kilometer) in the surrounding area (BBS 2021). The subsidence can have severe impacts on the lives and properties of the local residents. With the shortage of agricultural land in the region, the subsidence can further exacerbate the difficulties faced by the communities. The displacement of families and loss of crops and homes can cause significant economic and social hardships. Since 2008, the subsidence has persisted and continues to pose a threat to the area (Alam et al. 2022). To address these issues and safeguard the environment, it is imperative to investigate the area scientifically and propose effective remediation measures.

Though various researchers examined the subsidence of Barapukuria coal mine from different perspectives, no work has been done yet to analyze the pattern of subsidence and examine subsurface condition of the nearby habitats near the subsided zone. For example, Islam and Hayashi (2008) explored the area during 2008 when the subsidence began. However, the study was exploratory in nature based on coal bed methane and not focused on surface subsidence. Further, extensive research works were done by Howladar (2012, 2016) and Howladar and Hasan (2014). The focus of their research was to study the impact of coal mine on water and surrounding environment. In a relatively recent study, Arifeen et al. (2021) has examined the impact of mine on surrounding environments at Barapukuria highlighting the changes of land use and land cover. In another study, Alam et al. (2022) has simulated the mine induced subsidence using the displacement discontinuity method and indirectly discussed the potential danger for surrounding settlement area.

It is important to note that all of these studies focused on the impact of subsidence on water and the surrounding environment ignoring the directional trend and quantification of annual areal rate of subsidence. In addition, there is a dearth of research examining aerial extent of subsidence with regard to coal production. Apart from these, it is necessary to forecast that subsidence and explore the subsurface condition of nearby habitat areas and investigate whether they are at risk or not in the context of subsidence nature. This study aimed to fill this gap by comprehensively analyzing the subsidence and subsurface condition by utilizing both satellite imagery and resistivity methods. In fact, the integration of open-source satellite data and cost-effective, non-destructive resistivity surveys is a widely adopted approach worldwide (e.g., Indonesia, Malaysia, India, China, USA, Australia etc.) for studying various types of geohazards and conducting risk assessments (Singh et al. 2011; Kannaujiya et al. 2019; Muhammad et al. 2020; Widada et al. 2020).

Therefore, the objectives of this research were to comprehensively investigate the subsidence, including its trend, calculate the total areal extent and annual rate, forecast the future subsidence and investigate the subsurface condition of nearby villages to identify potential vulnerable zones integrating satellite data and resistivity methods. Analyses of subsidence regarding coal mining and subsurface condition in response provide crucial insights for designing and implementing effective strategies and planning for sustainable mine development as well as reducing geo-hazards.

Geological setup

The Barapukuria coal basin in NW Bangladesh is the country's first underground coal mine. Tectonically, the Barapukuria coal basin is located in the Rangpur Saddle of Bangladesh and is surrounded by the Himalayan Foredeep to the north, the Shillong plateau to the east, and the Indian Shield to the west (Alam et al. 2003). Geomorphologically, the surface above the coal basin seems like a flood plain basin with a 5 km² area, drained by the tributaries of the mighty river, Jamuna. Topographically, the region has low elevation, a gentle southward slope, and sits at an elevation of 30–36 m above mean sea level. Most of the land in the area is used for agriculture, primarily for growing rice (Islam and Hayashi 2008).

Geologically, the Barapukuria Basin is an asymmetrical north-south syncline (Fig. 1) containing Permian Gondwana coal-bearing sediments resting on an Archaean basement complex. The sequence mainly consists of continental arenaceous sediments, along with siltstones, shales, and up to six coal seams, reaching a thickness of up to 390 m. Subsidence along a major north-south fault in the Archaean basement, which also forms the eastern basin boundary, likely facilitated the formation of this sequence. The faults in the basin can be categorized as intra-basinal and boundary faults, as suggested by Bakr et al. (1996). The basin features numerous faults affecting the Gondwana sequence, with 37 faults identified through seismic interpretations (Hossain et al. 2020a, b). These faults typically occur in pairs, dipping towards the ESE. The Eastern Boundary Fault, spanning at least 5 km in an NNW-SSE direction, has significantly influenced basin sedimentation. It exhibits a westward displacement, affecting formations from the basement to the Tertiary age. This fault has a dip of 70–75 degrees towards the west, indicating a dominant dip-slip component and creating a half-graben type basin. Deposition thickness increases towards the east and southeast of the basin (Hossain et al. 2019). The stratigraphy of the Barapukuria Basin is mainly composed of Quaternary Alluvial deposits, Gondwana coal seams and the Precambrian Archean basement complex which is outlined in Fig. 2. An unconformable layer of the late Miocene/

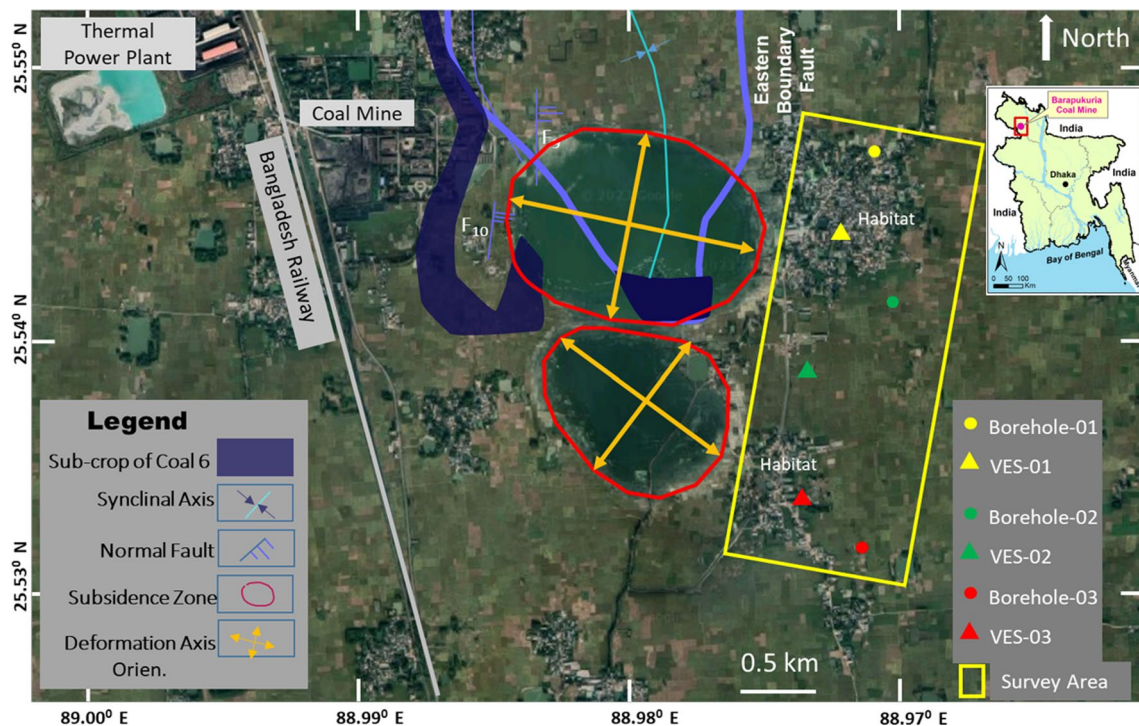


Fig. 1 Surficial features and the areal extent of the subsidence zone, and their orientation, along with the subsurface geological structure of the study area. Boreholes and geophysical vertical electrical sounding points in the surveyed area are used to assess the subsurface condition

Fig. 2 Stratigraphy of the study area indicated the stratigraphic position of coal seams with respect to other overburden and underburden formations [after Bakr et al. (1996)]

Maximum Thickness (m)	Lithology	Description	Formation	Age
1.83		Soil, Alluvium	Alluvium	Holocene-Recent
10.36	Clay		Modhupur Clay	Late Pliocene-Pleistocene
126.82		Sand, Silt and white clay	DupiTila	Late Miocene-Middle Pliocene
457.32		Coal sequence (Seam I to V)	Gondwana	Permian
14.32+	Diorite, Granite, Gneiss	Upper sandstone sequence of seam VI Seam VI Lower sandstone sequence of seam VI Tillites	Basement Complex	Archean

Pliocene Dupi Tila Formation conceals the basin entirely, with a thickness of 100–220 m.

Methodology

Vertical Electrical Sounding (VES) and Landsat satellite imagery are valuable tools for analyzing land subsidence and understanding its underlying causes (Singh et al. 2011; Widada and Saputra 2018; Kannaujiya et al. 2019; Muhammad et al. 2020; Widada et al. 2020). VES provides insights into the subsurface resistivity distribution at specific depths, allowing the identification of potential subsurface voids, compaction zones, or changes in groundwater levels that may contribute to land subsidence. On the other hand, Landsat satellite images offer a broader view of land surface changes over time, helping to detect large-scale subsidence patterns and land use alterations. By combining VES data with Landsat imagery, a comprehensive understanding of the spatial distribution, trends, and contributing factors of land subsidence can be achieved, ultimately aiding in risk assessment and effective planning to combat the situation.

Satellite images and VES surveys were used to identify the surface and subsurface vulnerable zones. In fact, the satellite images can give us a potential clue to detect change and trend due to land subsidence from which we can project the potential vulnerable zone (Widada et al. 2020). Subsurface zones are actually vulnerable or not can be assessed further by electrical resistivity method (Widada et al. 2020). The flowsheet of the conceptual methodology applied in this research work is shown in Fig. 3.

Satellite image analysis

Satellite time series data are used to identify changes in the landscape over time period (Sidhu et al. 2018). It is also used in this research to identify the nature and trend of subsidence over time. Due to availability of long-time satellite data sets as open source, we collected Landsat-7 ETM+ (Enhanced Thematic Mapper Plus) and Landsat-8 OLI (Operational Land Imager) data at the month of November and December from 2005 to 2020 having 30 m and 16 day spatial and temporal resolution, respectively. During these periods, cloud free and apparently clear images were found. The

Fig. 3 Workflow shows the different steps used in this study

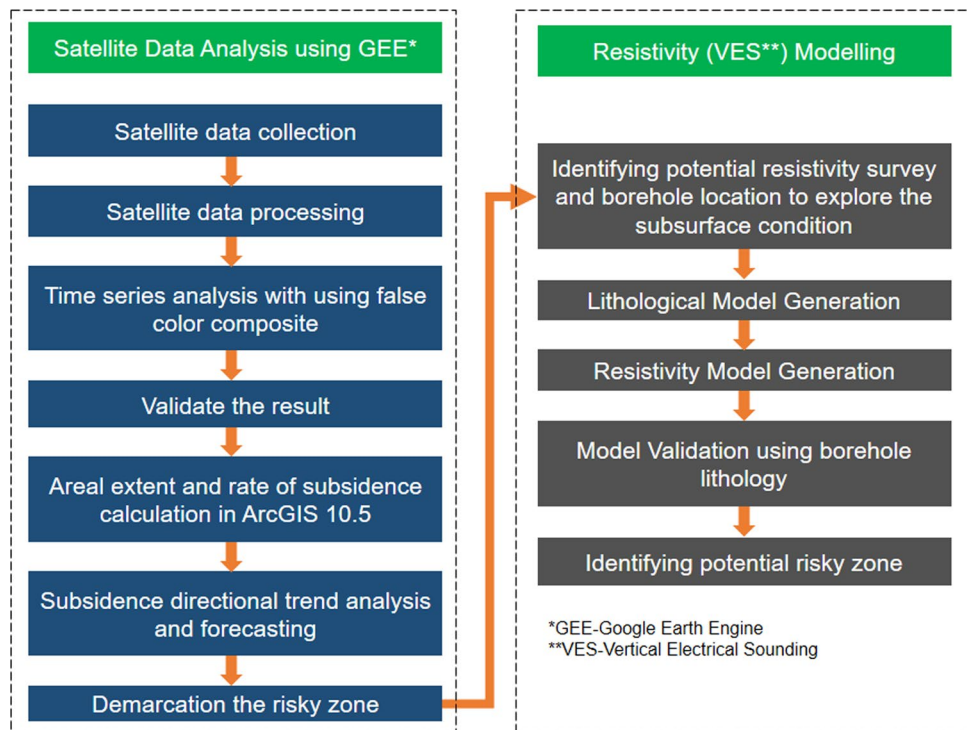


Table 1 Specification of satellite data used for the investigated area

Satellite	Sensor	Path/row	Year of acquisition	Spectral bands	Resolution (m)	Cloud cover
Landsat-7	ETM +	138/042	2005–2013	8	30	< 5%
Landsat-8	OLI	138/042	2014–2020	11	30	< 5%

specification of the satellite data used in the research work is shown in Table 1.

The Landsat satellite images were fetched from the website of the United States Geological Survey (USGS) (<https://earthexplorer.usgs.gov/>) by google earth engine, a cloud-based platform for geospatial analysis (Gorelick et al. 2017; Xiong et al. 2017). To effectively use remotely sensed data for change detection, various methods are available (Lu et al. 2004; Zhu 2017). We used the multiday false color composite image comparison method to detect land cover changes visually using multi-temporal satellite images which consider texture, shape, size, and patterns of the images to identify land use and land cover (LULC) changes effectively (Martin 1989; Patra et al. 2006; Xu and Chen 2012; Imam 2019). As we have the study area's knowledge and familiarity from field visit, this technique works as a fast and economical way to identify our target zone and detecting changes annually. All the maps were assigned to the WGS1984 UTM Global Geodetic Coordinates System.

All the images were processed using google earth engine and later in GIS platform, involving geometric and radiometric enhancement, mosaicking, and sub-setting of different Landsat sensors. In order to improve the precision of change detection using the multiday image comparison method, additional high-resolution Landsat-8 OLI satellite images from the years 2014 to 2020 were incorporated (Tiwari and Saxena 2011; Kaul and Sopan 2012; Rawat and Kumar 2015). Moreover, ESRI landcover and Dynamic World landuse landcover maps and existing scientific reports were integrated to validate and verify the obtained results (Brown et al. 2022; Chaaban et al. 2022). To calculate the aerial extent of the subsided area annually, we employed an indirect visual analysis method in ArcGIS 10.5 version after georeferencing the images (Martin 1989; Choudhury et al. 2012; Dang et al. 2021). The accuracy of the measured values was validated through direct field visits for the last three years (2018–2020), while the aerial extent of subsidence values was validated using previously published landcover maps, reports and journals (Arifeen et al. 2021; Brown et al. 2022; BCMCL 2023).

Subsequently, we determined the annual rate and trend of subsidence from the images and employed statistical linear regression to extrapolate the aerial extent of subsidence for the next ten years, estimating the vulnerable area of future subsidence. The trajectory direction of subsidence and the potential risky zone were identified using visual graphics, and accordingly, a vertical electrical resistivity survey was conducted in the area to explore the subsurface conditions near habitats where thousands of people reside.

Surface electrical resistivity

Based on the trajectory of areal extent of subsidence to identify potential risky zones, we conducted a vertical electrical resistivity survey in the study area. This survey aimed to explore the subsurface condition of nearby habitats where thousands of people reside. We used three vertical electrical resistivity (VES) profiles at the habitat areas to explore where land subsidence is likely to occur and to what extent. Though this method is comparatively old, it is still very effective and reliable for exploring subsurface conditions (Widada et al. 2019; Ulfah et al. 2021). Moreover, previous studies found 90% reliability for identifying subsurface geology in the sedimentary environment of Bangladesh using this method (Rahman and Woobaidullah 2020).

The resistivity survey was conducted in the field according to the standard method of ASTM D6431 (2010). Preliminary location of survey lines was investigated with the aid of satellite image and on-site visit was conducted to justify the location and enough accessibility to cover whole study area. The survey line was oriented perpendicular to the land subsidence trend, extending 500 feet to investigate subsurface conditions up to 200 feet deep. Subsurface anomalies, such as cracks, faults, or other irregularities, result in abrupt increases in resistivity, signaling potential anomalous zones (Wenner 1916). It is crucial to note that subsurface geological layers, porosity, compaction, and other factors significantly influence resistivity (Woobaidullah et al. 2016). Given the presence of clay and sandy layers in the survey area, this method effectively distinguishes between vulnerable and non-vulnerable zones. By applying this approach, we can accurately assess the vulnerability of subsurface concerning the vertical depth influenced by the subsidence trend.

Schlumberger array was used as it is less susceptible to contact resistance and nearby geologic conditions that may affect readings and slightly faster in field operations, since most of the time the current electrode is moved between readings (Woobaidullah et al. 2020). All things were taken into consideration, which may cause noise during the

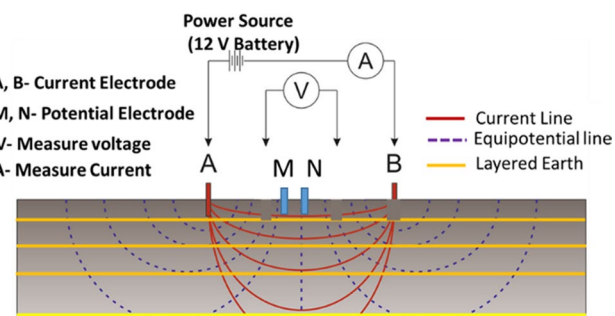


Fig. 4 Vertical electrical sounding (VES) layout for field survey (ASTM D6431 2010)

measurements and could influence the output. For instance, before the survey at each location, contact resistance was checked in order to get a greater signal-to-noise ratio. In fact, the resistivity of sub-soil is affected by soil composition, moisture content, and temperature.

During data acquisition, we positioned four electrodes symmetrically in a straight line (Fig. 4) to ensure good contact with the subsurface. We progressively increased the current electrode spacing to improve vertical depth resolution while keeping the potential electrode spacing constant. It is important to note that if the ratio of current electrode spacing to potential electrode spacing is too short, it can impact potential difference measurement accuracy (Khalil 2020).

To address potential distortions caused by lateral heterogeneity and equipment failures, we used an updated resistivity meter, the McOHM (Model-2115, OYO Corporation, Tokyo, Japan, Digital Electrical Prospecting System). This robust device integrated the transmitter and receiver, enhancing signal-to-noise ratio with its built-in stacking processing function. It automatically recorded and digitally displayed results during data collection, ensuring accuracy (Thabit and Al-zubedi 2015). We followed a similar procedure to collect data from all other points in the study area.

Like all other geophysical methods, resistivity method faces some ambiguities. Borehole logging data were used for calibration of the resistivity results to overcome these ambiguities (ASTM D6431 2010). Borehole and VES survey location were much closer to borehole location for comparison and calibration (Fig. 5). IX1D open source software was used for processing resistivity sounding data and

utilized Rockworks 17 commercial software for lithology and resistivity modelling. Local geology, geomorphology and hydrogeological conditions were focused to reduce the interpretation ambiguities arising from equivalence of the resistive layers and their thickness. Previous published reports and articles were also used to justify our interpretations (Woobaidullah et al. 2016, 2020).

Results

Satellite data analysis

Since the commencement of subsidence, the area had been consistently filled with water. As a result, a false-color composite image utilizing the SWIR, NIR, and Red bands was employed to classify the images into two distinct features. The feature of interest, indicative of the formation of a substantial water pool due to subsidence, appeared as a distinctive blue color. In contrast, the remaining features within the research area appeared as black pixels (Fig. 6). Upon careful examination of the classified image generated from the false-color composite, it revealed that no subsidence observed till 2007 since the beginning of commercial mining operations in 2005. However, subsidence began primarily in 2008 and areal extent of subsidence was 4.9 acres (Table 2) and by 2010, a double subsidence zone formed, whereas the northern zone being smaller in comparison with the larger southern zone (Fig. 6).

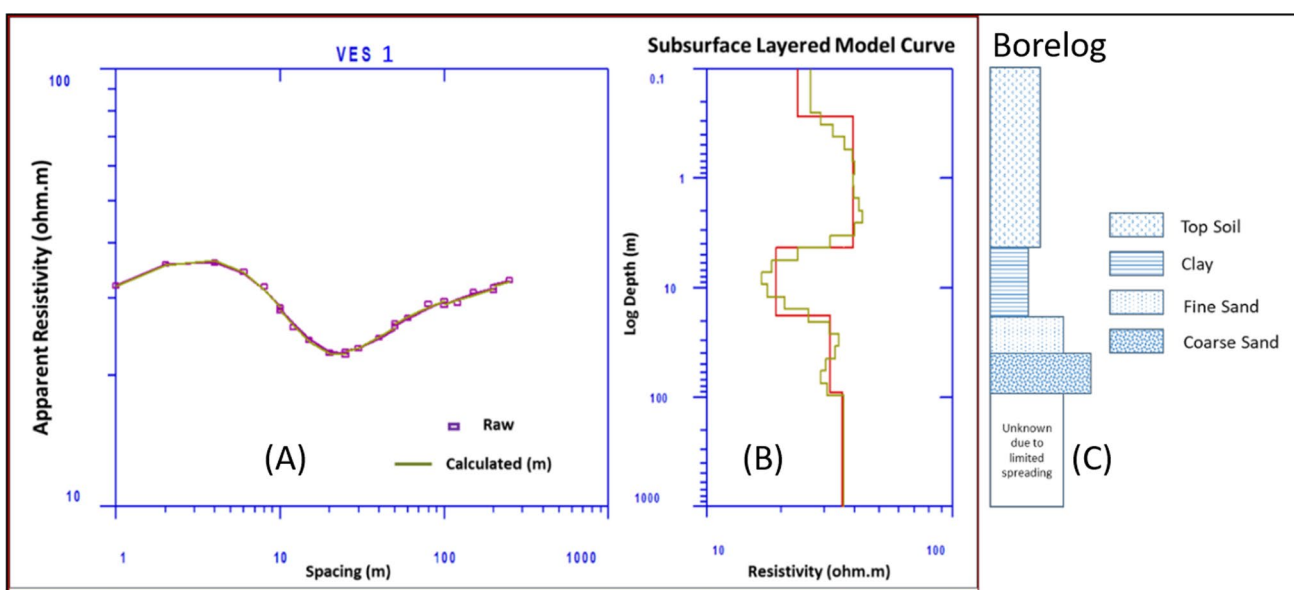


Fig. 5 Calibration of VES model with lithological model. **A** Raw data collected from field and curve fitting. **B** Subsurface layered model curve along with apparent resistivity and thickness. **C** Borehole lithology which is closely in line with the resistivity layered model

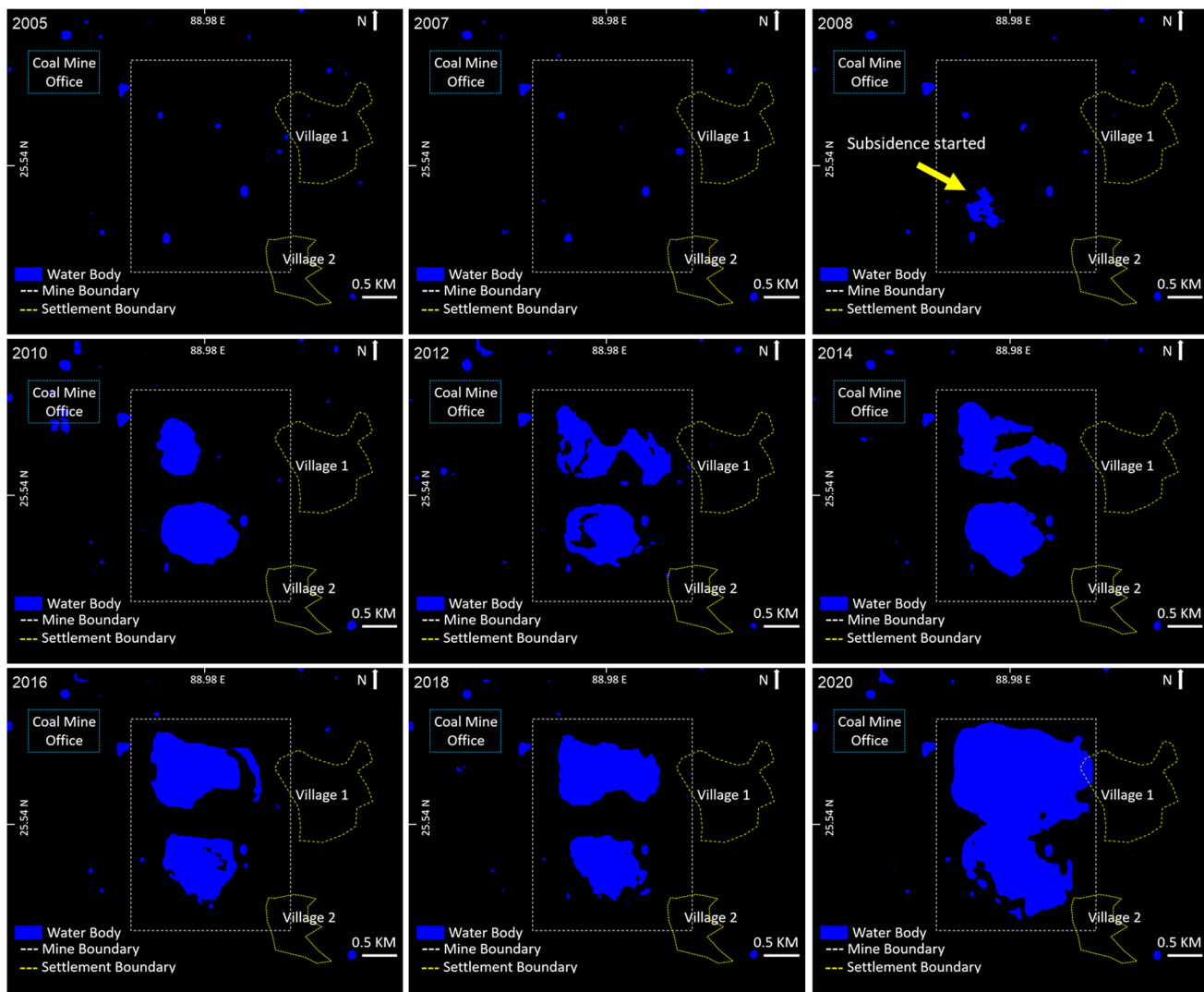


Fig. 6 Annual land subsidence time lapse images from 2005 to 2020 were generated using a multiday three-band false color composite (SWIR, NIR, Red) of the Barapukuria coal mine area. Images were

collected in the month of December each year and calibrated using field visits and high-resolution satellite imagery

Over the subsequent years, subsidence continued to increase in a linear fashion. By the year 2020, the two subsidence zones had merged (Fig. 6), resulting in a total subsided area of 214 acres (Table 2). This represented a significant increase, exceeding 40-fold when compared to the subsidence area observed in 2008. The aerial extent of subsidence over this period was calculated using the ArcGIS 10.5 platform, after proper georeferencing of the images. The results obtained were subsequently validated through comparisons with ESRI and Dynamic World Landcover maps (Fig. 7).

After carefully analyzing the images, it revealed the continuity of aerial extent and an alarming trend of subsidence

pattern for the study area that has developed since the beginning of subsidence in 2008. Image analysis conducted from 2008 to 2020 clearly indicates that the subsidence area was nearly oval in shape and its trend was west to east direction (Fig. 6). Table 2 data consistently showed a progressive increase in the cumulative subsided area, reflecting a gradual expansion of land subsidence in the region over the years. This trend aligns with observations from satellite data spanning 2008 to 2020. However, individual yearly subsidence areas exhibited variability, with certain years experiencing significant subsidence, such as 33.8 acres in both 2015 and 2016, 45 acres in 2020 while others witnessed

Table 2 Time series data of total subsidence, annual subsidence and coal production

Year	Cumulative area of subsidence (acres)	Individual year subsided area (acres)	Annual production (lakh MT)*
2008	4.9	4.9	8.4
2009	12.3	7.4	7.15
2010	27.6	15.3	6.5
2011	30.9	3.3	8.5
2012	44.9	14	8.6
2013	59.15	14.25	9.65
2014	73.4	14.25	6.8
2015	107.2	33.8	10.25
2016	141	33.8	11.6
2017	151	10	9.23
2018	163	12	8.05
2019	169	6	8.11
2020	214	45	7.54

*Source: BCMCL (2023)

minor subsidence, e.g., 4.9 acres in 2008 and 3.3 acres in 2011.

From the correlation (Fig. 8), it is prominently seen that the cumulative subsided area increased linearly with time and their correlation coefficient was nearly perfect (0.98) in nature. However, surprisingly, no significant correlation (0.34) found between annual coal production and individual year subsidence. In addition, an insignificant correlation (0.23) found between total subsided area and annual coal production.

The rate of subsidence was notably higher (17.4 acres per year) (Fig. 9), and predictions based on the annual rate of areal extent using linear regression for next 10 years suggest that the subsided area will be nearly doubled (405 acres) by 2030 (Fig. 10).

Resistivity data analysis

Based on the forecasted trajectory of subsidence derived from linear regression (Fig. 10A), vertical electrical sounding survey conducted in the extrapolated risky zones (Figs. 1 and 10B) which revealed four distinct lithological units (clay, mixed clay and sand, fine sand, and coarse sand layers). The borelogs and VES results closely agreed with each other where the thicknesses of the layers were generally consistent (Table 3). The lithological profile showed the vertical and horizontal distribution of subsurface lithology of the two nearby villages (Fig. 11) which demonstrated that sand layer was sandwiched between two clay layers.

The resistivity distribution of subsurface layers from VES survey helps to assess the existence of vulnerable

zones (Fig. 12). The resistivity section along N–S direction revealed a striking contrast in resistivity between the southern and northern parts of the study area. Most importantly, the northern part of the study area at 60–100 feet depth showed relatively higher resistivity (80–90 Ω.m) compared to the southern part (20–80 Ω.m) having subsurface extent of 1 km demonstrating significant anomaly below the surface.

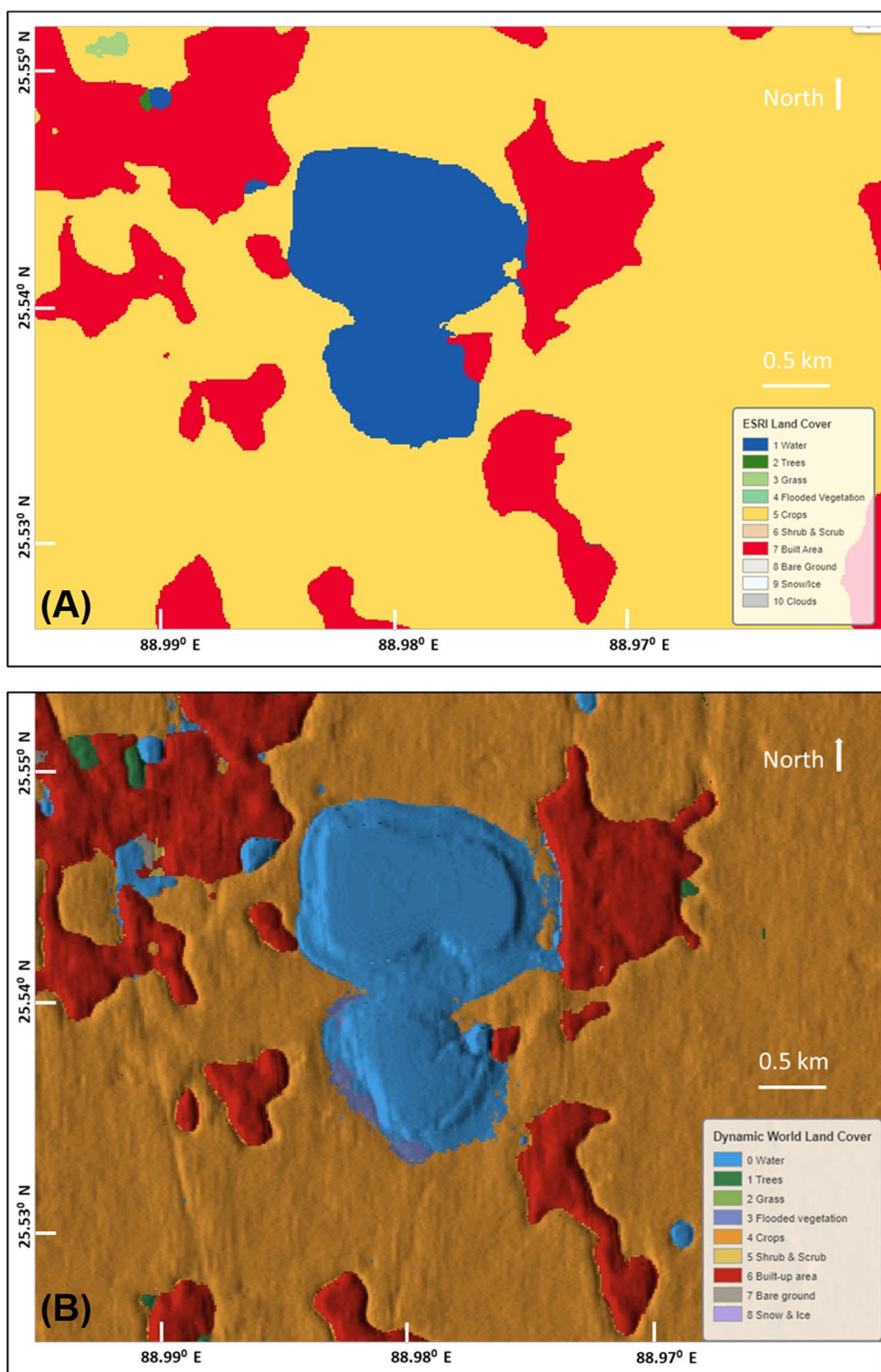
Discussion

This research aimed to provide a more robust understanding of mine-induced subsidence and associated risk in the Barapukuria coal mine and its surrounding. The results from this study showed a pronounced west-to-east directional trend, towards the nearby residential areas (Fig. 6), revealing an eastward inclination of the underlying geological layers. Previous research indicates the complexity of the subsurface characteristics, marked by various faults, lineaments, and an identified asymmetrical synclinal structure within seismic sections (Islam and Hayashi 2008). Notably, the crucial insight emerges from Alam et al. (2022), shows that the fold's axis aligns in a north–south direction, with its sloping side tilting towards the east. This arrangement likely explains the possible reason of orientation of subsidence towards the east. Using displacement discontinuity method, he concluded that the role of fault and dykes is negligible for subsidence at Barapukuria where subsurface tilted strata and strain factors mainly plays a vital role for subsidence. He also doubted in his research about the future vulnerability of nearby villages and coal mine and recommended backfilling and other methods to adopt to manage the situation.

The subsidence phenomenon exhibited an approximately oval shape, which reflects the variations in lithology of overburden and bedrock and the flat coal seams. This observation aligns with a recent theoretical analysis conducted by Yan et al. (2021) concerning mine-induced overburden subsidence in horizontal coal seams in Mongolia. He deduced that variations in lithology and properties between the overburden and bedrock lead to the formation of three-dimensional bowl or two-dimensional oval like shape of the subsidence area.

The continuous extension as well as the alarming rate (17.4 acres per year) of the phenomena further suggest that the subsurface layer is composed less competent rocks which are vulnerable to subsidence. Research suggests that the less competent coal-bearing formation of Barapukuria stratigraphically existing below the Dapi Tila water-bearing formation, naturally vulnerable to subside (Howladar 2016). In addition, the stratigraphy of the study area formed under river deltaic condition (Hossain et al. 2020a, b) and recent study revealed that coastal plains and river deltaic regions are highly prone to frequent land subsidence, accounting for

Fig. 7 Land use–land cover map
A ESRI and **B** World Dynamic
 to validate the areal extent of
 subsidence



around 47% of 290 study areas worldwide (Bagheri-gavkosh et al. 2021). The possible other factor responsible for the continuous extension of subsidence area is the overexploitation of ground water. Bagheri et al. (2021) found that human activities are responsible for 76.92% of all land subsidence cases, with groundwater extraction being the primary

contributor, accounting for 59.75% of these cases (Bagheri et al. 2021). They also showed a strong and direct correlation between the average land subsidence rate and groundwater withdrawal ($R^2=0.950$) as well as groundwater level decline ($R^2=0.888$). In fact, 14 deep tube wells are continuously in operation to cool the thermal power plant located near the

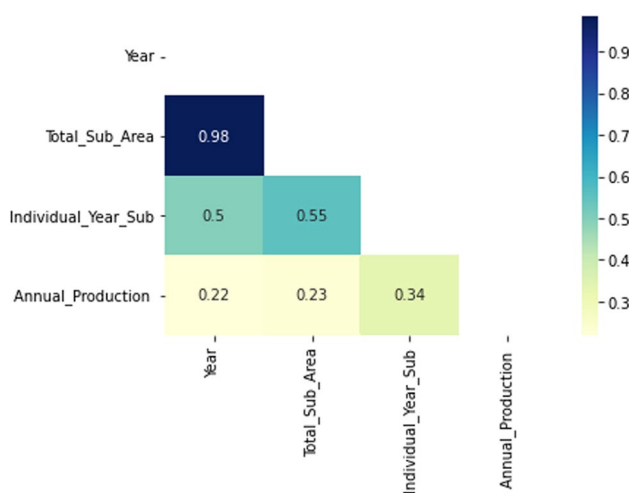


Fig. 8 Correlation coefficient among different variables

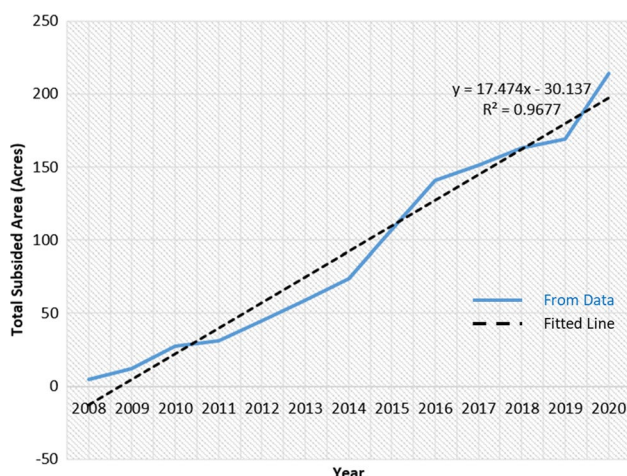


Fig. 9 Observed and simulated subsidence at Barapukuria

Barapukuria coal mine (Sunny 2018). As a result, low permeable clay may deform, compact and eventually subside.

The present study provides a significant insight into the relationship between subsidence and coal production in the study area over a 13-year period. Quite surprisingly, we didn't find any significant statistical correlation between annual coal production and areal extent of subsidence (Fig. 8). Despite some years a larger subsided area corresponded with lower production, a clear and consistent relationship between the two variables was not established. However, it possibly indicates that other factors are responsible for the continuous aerial extent of subsidence in the area. Given that Ghazifard et al. (2017) found that subsidence is influenced by factors like sediment properties (type, thickness, stiffness, and compressibility), geological history, coal basin structure, hydrogeology, mining method, and the presence of multiple coal seams.

From borehole and VES survey we deciphered the subsurface lithology of the nearby villages mainly composed of sand, clayey sand and sand, which are more prone to subsidence. This finding is congruent with the recent study conducted in Malaysia which showed that Holocene deposits in river deltaic regions are naturally soft and more prone to subsidence (Widada et al. 2018, 2019). They concluded that the presence of mechanically unstable clay/sandy clay layers of Holocene age is susceptible to compression contributing to substantial land subsidence.

Based on the east ward direction of surficial extent and the forecasted trajectory of subsidence, the conducted VES survey revealed a notable high-resistivity zone in the northern region of the area, coinciding with the presence of the thickest layers of alluvial sediments that possess a higher consolidation potential (Widada et al. 2018). Furthermore, the northern part of the area is characterized by a denser population compared to the southern part (Arifeen et al. 2021). One plausible explanation is that this denser population, coupled with overexploitation of groundwater and the ongoing trend of subsidence expansion, may lead to subsurface conditions deteriorating due to layer compaction, resulting in increased resistivity. It may also reflect differential compaction of different hydrostratigraphic unit of Holocene alluvial deposits. Our findings are supported by previous study conducted by Howlader (2014). He reported that groundwater is declining in this area day by day causing the decrease of porosity and permeability leading compaction of subsurface layers which eventually give higher resistivity value than the surrounding zone. Further, extraction of groundwater by the nearby thermal power plant exacerbates this condition.

Moreover, in the field visit we found shattered walls and cracked yards in the northern part of the study area shown in Fig. 13. Since the coal extraction, several villages near the mining area (Moupukur, Jigagari, Sardarpara, Kalupara, and Bashpara) have experienced land subsidence while excavation activities resulted in cavities formation (Sunny 2018). Therefore, from the survey and field photo observation, it reflects some crucial evidence that the habitat of the northern part (Patrapara) is more vulnerable to geohazard in near future.

The geophysical data also indicates that the same layer in the southern part of the study area does not currently display any anomalous resistivity values. This may be due to a less pronounced trend of expansion of subsidence and urban development in the southern region. However, it is important to note that in the future, the southern part may also be influenced by similar conditions. Alternatively, it may be other unknown factors which may cause normal resistivity below the surface at that particular depth in the southern part of the study area. However, further work is needed to unravel the subsurface scenario in detail incorporating other direct and

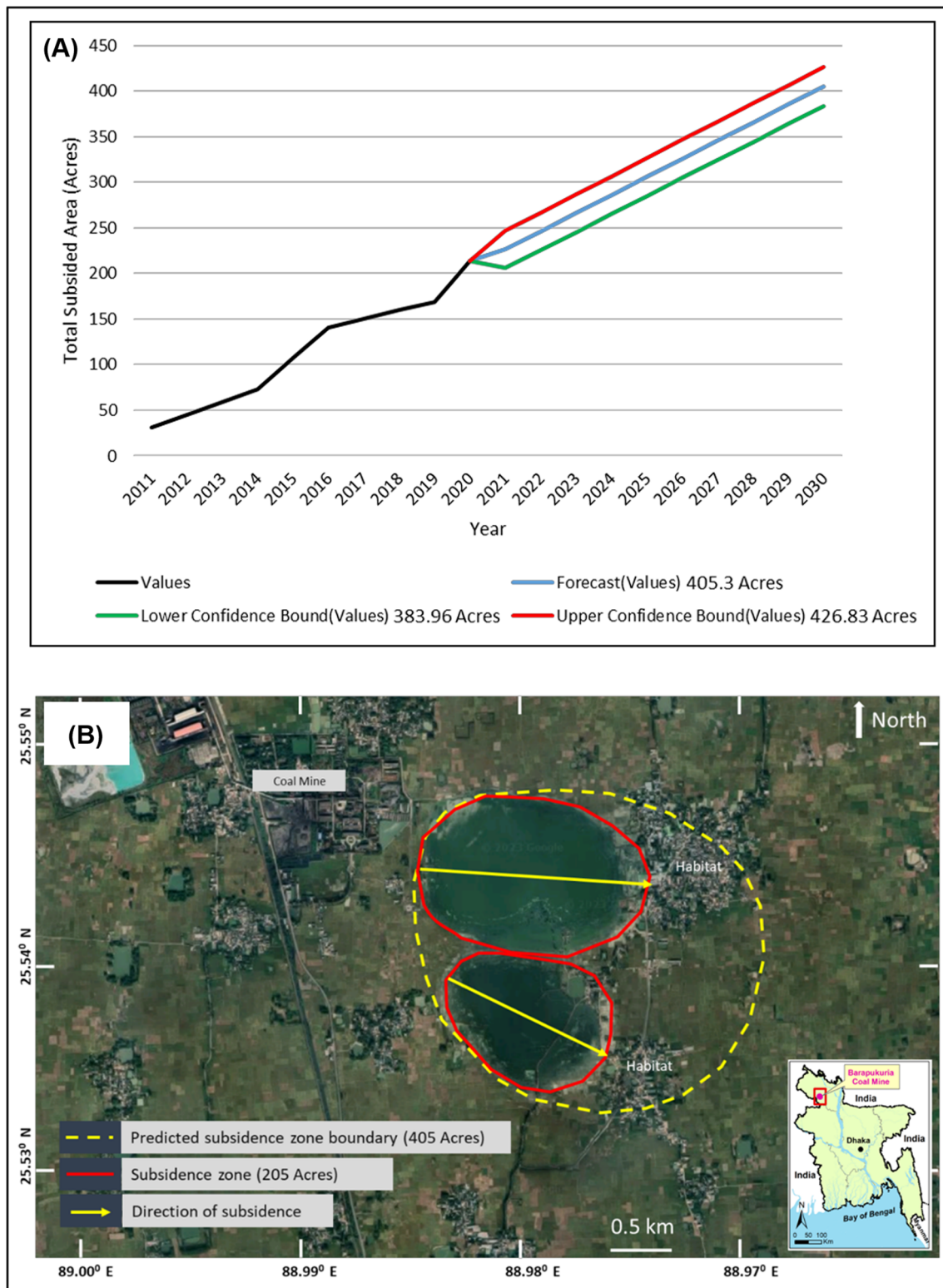
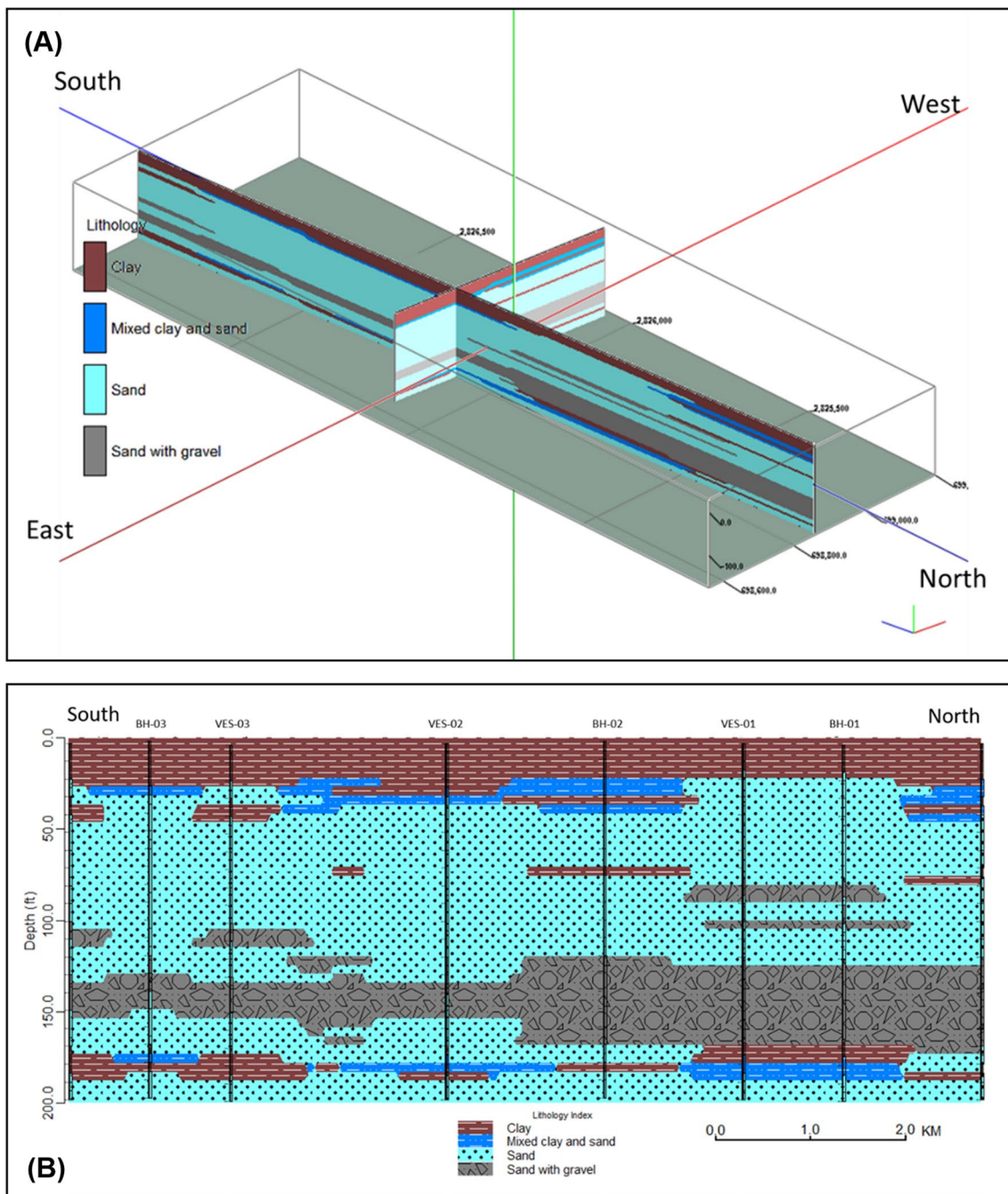


Fig. 10 Map showing **A** forecasting subsidence for different bound values in Barapukuria, **B** the existing and forecasted subsidence zones in Barapukuria

Table 3 Comparison of borelogs and VES data

Lithology from Borelogs	Borehole thick-ness (feet)	Lithology from VES	VES thickness (feet)	Resistivity (ohm-m)
Clay	30–40	Top soil	0.5–13	5–20
Mixed Clay and Sand	5–10	Clay	15–40	2–12
Fine sand	80–100	Fine sand	60–100	10–110
Coarse sand	30–50	Coarse sand	40–50	20–50

**Fig. 11** Borelog-derived **A** lithological fence diagram, and **B** lithological cross section along north–south direction of the study area

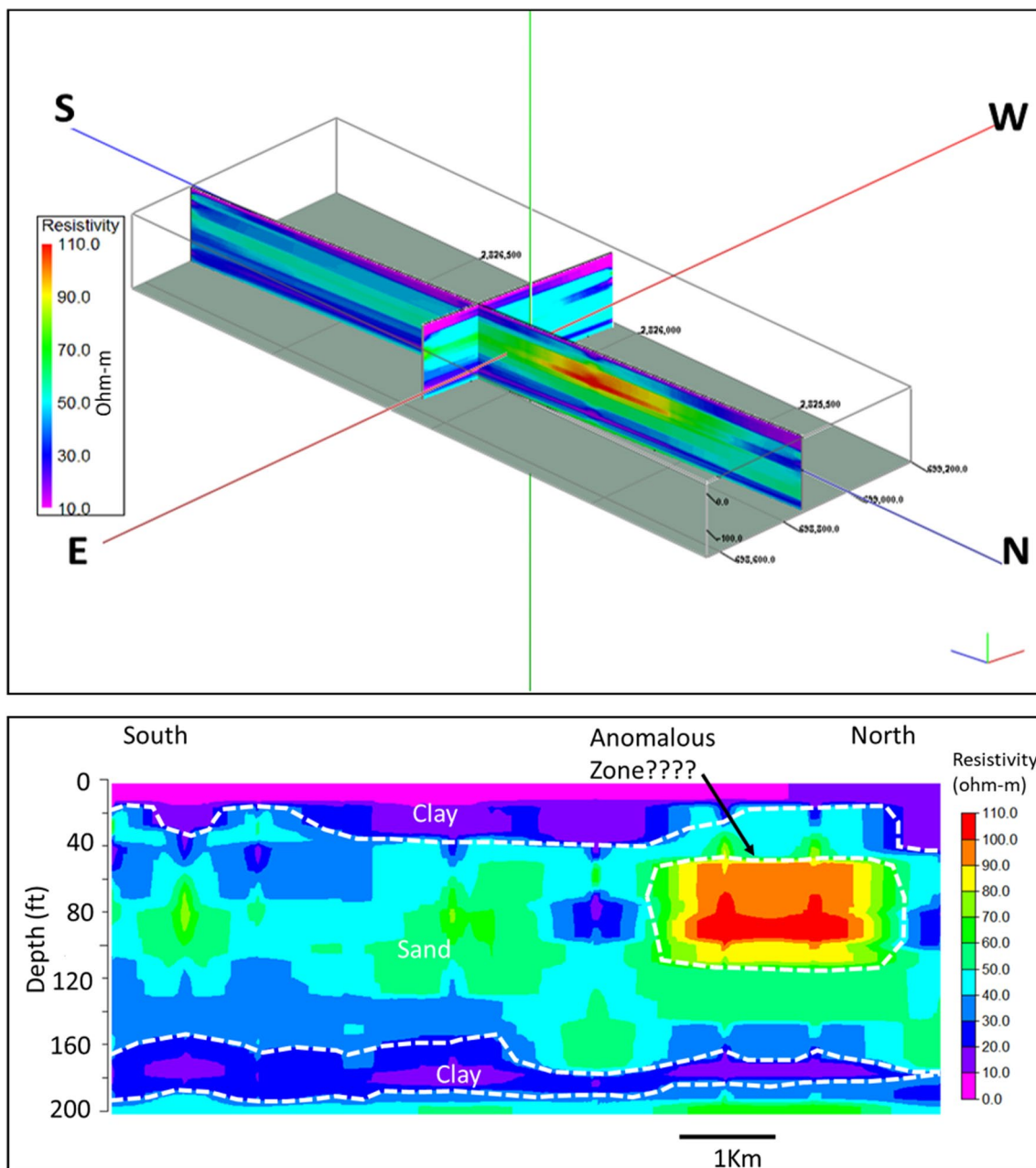


Fig. 12 Resistivity survey derived **A** fence diagram and **B** cross section along N–S of the study area

indirect geological and geophysical methods for confirmation the scenario. Given the recent plan to extend the northern part of the coal mining area (“Barapukuria coal mine” 2021), it is crucial that policy makers take these findings into consideration to assess the vulnerability of the subsurface in detail and take action to rehabilitate affected communities. Further, this issue should be taken into consideration for future exploration of other 4 coal fields in Bangladesh.

Limitations and future research directions

While this study offers valuable insights, it has limitations that can guide future research. These include a limited number of boreholes and VES surveys, which should be expanded in future studies. To advance our understanding, future research should employ a broader range of geological and geophysical methods for detailed subsurface analysis in sustainable mine development.



Fig. 13 Surface cracks and shattered walls found during the field visit in the northern part of the study area

Nevertheless, this study's key contribution lies in its comprehensive analysis of Barapukuria's subsidence phenomena, including trend forecasting. This research significantly enhances our understanding about the expanding subsidence issue, aiding regional planning and development. In addition, through geophysical and borehole data analysis, we have identified the subsurface areas at risk of geohazards related to land subsidence. We expect our findings will empower the decision makers for informed decision-making and proactive mitigation measures against the impact on human activities and infrastructure. Furthermore, integrating these methods into natural disaster research holds promise for global studies in the future.

Conclusions

In this study, we analyzed the land subsidence in the Barapukuria coal mine as well as investigate the subsurface zone to assess the risk through the integration of satellite and resistivity methods. The analyses enabled us to comprehensively understand the alarming rate (17.4 acres per year) and west-to-east trend of surficial extent of land subsidence directed towards the nearby habitats along with forecasting future subsidence area, which will helpful for the sustainable mine design, and planning regional development of the study area. Particularly, this study helped in identifying subsurface zone of nearby habitat that is highly prone to geohazards associated with land subsidence. Furthermore, this study identified subsurface layers which are essentially Holocene deposits composed of clay,

clayey sand and sand. In fact, the layers are incompetent in nature and may undergo a rapid land subsidence in near future. Therefore, our results highlight the need for immediate actions for the alarming annual rate of surficial areal extent of subsidence and vulnerable subsurface condition of adjacent living areas to rehabilitate the people by the authorities.

Acknowledgements The authors thank the authority of the Bangladesh Council of Scientific and Industrial Research (BCSIR) for approving the Research and Development Project for the fiscal years 2020–2021 having Reference No. 39.02.0000.011.14.128.2020/636, Serial-65, Unit Code-IMMM-01. The authors also express their gratitude to anonymous reviewers for their constructive comments to improve the manuscript.

Author contributions MISH: conceptualization, field investigation, formal analysis, statistical analysis, original manuscript writing, project administration, methodology, data curation, visualization, software. MSA: field visit and calibration of data. PKB: supervision, project administration. MSR: review of the original draft of manuscript and editing, map preparation, manuscript formatting. MSS: valuable feedback during field work. MNZ: fund manage, project administration. MAS: conceptualization, manuscript reviewing and editing, MJR: conceptualization, writing—review and editing, supervision. ASMW: fund manage, writing—review and editing, supervision.

Funding Financial support was received from Bangladesh Council of Scientific and Industrial Research (BCSIR), Ministry of Science and Technology, Bangladesh, for conducting this study.

Availability of data The data are available on request.

Code availability The code is available on request.

Declarations

Conflict of interest The authors declare that there is no conflict of interests regarding publishing of this paper.

References

- Abubakar S, Abir IA, Muhammad SB, Mohammed A (2020) Land subsidence studies of seberang perai Malaysia, by integrating remote sensing technique and resistivity survey method. *IOSR J Appl Geol Geophys* 8(1):41–47 <https://doi.org/10.9790/0990-0801034147>
- Abubakar S, Shanmugaveloo AAL (2021) Surface deformation studies in South of Johor using the integration of InSAR and resistivity methods. *Caliphate J Sci Technol* 2021(2):167–172.
- Alam M, Alam MM, Curray JR, Chowdhury MLR, Gani MR (2003) An overview of the sedimentary geology of the Bengal Basin in relation to the regional tectonic framework and basin-fill history. *Sed Geol* 155(3–4):179–208. [https://doi.org/10.1016/S0037-0738\(02\)00180-X](https://doi.org/10.1016/S0037-0738(02)00180-X)
- Alam AKMB, Fujii Y, Eidee SJ, Boeut S, Rahim AB (2022) Mining-induced subsidence prediction by displacement discontinuity method: a case from Barapukuria longwall coal mine Bangladesh. *Sci Rep* 12(1):14800. <https://doi.org/10.1038/s41598-022-19160-1>

- Arifeen HM, Chowdhury MS, Zhang H, Suepa T, Amin N, Techato K, Jutidamrongphan W (2021) Role of a mine in changing its surroundings—land use and land cover and impact on the natural environment in barapukuria, bangladesh. *Sustainability (Switzerland)* 13(24):13602. <https://doi.org/10.3390/su132413602>
- ASTM D6431 (2010) Standard guide for using the direct current resistivity method for subsurface investigation. ASTM International, West Conshohocken. <https://doi.org/10.1520/D6431-99R10.2>
- Bagheri-gavkosh M, Mossa S, Ataei-ashtiani B, Sohani Y (2021) Land subsidence: a global challenge. *Sci Total Environ* 778:146193. <https://doi.org/10.1016/j.scitotenv.2021.146193>
- Bakr MA, Rahman QMA, Islam MM, Islam MK, et al (1996) Geology and coal deposits of Barapukuria Basin, Dinajpur District, Bangladesh. Records of Geological Survey of Bangladesh, Vol. 8 (Part 1)
- Barapukuria Coal Mine (2021) Barapukuria coal mine expanding northward. The Daily Star. <https://www.thedailystar.net/country/news/barapukuria-coal-mine-expanding-northward-2114077>. Accessed on 20 June 2021
- BBS (2021) Statistical Pocketbook 2020. Bangladesh Bureau of Statistics, Statistics and Informatics Division, Ministry of Planning, Government of the People's Republic of Bangladesh. https://bbs.portal.gov.bd/sites/default/files/bbs.portal.gov.bd/page/d6556cd1_dc6f_41f5_a766_042b69cb1687/2021-06-30-09-25-67bbe4c5c15d7773d82c86adbd26bba9.pdf. Accessed on 13 Aug 2021
- BCMCL (2023) Annual Report 2021–2022, Barapukuria Coal Mine Company Limited, Dinajpur, Bangladesh. https://bcmcl.org.bd/sites/default/files/files/bcmcl.portal.gov.bd/annual_reports/a351e5a3_8219_4a8a_b3f1_d0d1c5fbe7da/2023-04-06-08-17-1c35ef561d07742cb831d50219bd5ea1.pdf. Accessed on 08 March 2023
- Brown CF, Brumby SP, Guzder-Williams B, Birch T et al (2022) Dynamic world, near real-time global 10 m land use land cover mapping. *Sci Data* 9(1):1–17. <https://doi.org/10.1038/s41597-022-01307-4>
- Chaabani F, El Khattabi J, Darwiche H (2022) Accuracy assessment of ESA WorldCover 2020 and ESRI 2020 land cover maps for a region in Syria. *J Geovis Spat Anal*. <https://doi.org/10.1007/s41651-022-00126-w>
- Choudhury I, Chakraborty M, Santra SC, Parihar JS (2012) Methodology to classify rice cultural types based on water regimes using multi-temporal RADARSAT-1 data. *Int J Remote Sens* 33(13):4135–4160. <https://doi.org/10.1080/01431161.2011.642018>
- Del Conte S, Falorni G (2019) InSAR monitoring of subsidence induced by underground mining operations. Proceedings—Rapid Excavation and Tunneling Conference, 2019-June. p 399–407. https://doi.org/10.36487/acg_rep/1815_54_falorni
- Dang VK, Nguyen TD, Dao NH et al (2021) Land subsidence induced by underground coal mining at Quang Ninh, Vietnam: persistent scatterer interferometric synthetic aperture radar observation using sentinel-1 data. *Int J Remote Sens*. <https://doi.org/10.1080/01431161.2021.1875513>
- Ghazifard A, Akbari E, Shirani K, Safaei H (2017) Evaluating land subsidence by field survey and D-InSAR technique in Damaneh city. *Iran J Arid Land* 9(5):778–789. <https://doi.org/10.1007/s40333-017-0104-5>
- Gorelick N, Hancher M, Dixon M et al (2017) Google earth engine: planetary-scale geospatial analysis for everyone. *Remote Sens Environ* 202:18–27. <https://doi.org/10.1016/j.rse.2017.06.031>
- Hossain MS, Khan MSH, Chowdhury KR, Abdullah R (2019) Synthesis of the tectonic and structural elements of the bengal basin and its surroundings. *Springer Geology (Issue January)*. Springer, New York. https://doi.org/10.1007/978-3-319-99341-6_6
- Hossain MS, Xiao W et al (2020a) Geodynamic model and tectono-structural framework of the Bengal Basin and its surroundings. *J Maps* 16(2):445–458. <https://doi.org/10.1080/17445647.2020.1770136>
- Hossain MS, Khan MSH, Abdullah R, Chowdhury KR (2020) Tectonic Development of the bengal basin in relation to fold-thrust belt to the east and to the north. Springer, New York, pp 91–109. https://doi.org/10.1007/978-3-030-40593-9_4
- Howladar MF (2012) Coal mining impacts on water environs around the Barapukuria coal mining area, Dinajpur, Bangladesh. *Environ Earth Sci.* 70(1):215–226. <https://doi.org/10.1007/S12665-012-2117-X>
- Howladar MF (2016) Environmental impacts of subsidence around the Barapukuria coal mining area in Bangladesh. *Energy Ecol Environ* 1(6):370–385. <https://doi.org/10.1007/s40974-016-0031-x>
- Howladar MF, Hasan K (2014) A study on the development of subsidence due to the extraction of 1203 slice with its associated factors around Barapukuria underground coal mining industrial area, Dinajpur, Bangladesh. *Environ Earth Sci* 72(9):3699–3713. <https://doi.org/10.1007/s12665-014-3419-y>
- Imam E (2019) Remote sensing and GIS module: colour composite images and visual image interpretation. University Grand Commission (UGC), MHRD, Government of India.
- Islam MZ, Chakraborty P (2021) Importance of failure modes and effect analysis application for risk analysis in Barapukuria coal mine, Bangladesh. *Int J Innov Eng Res Technol.* 8:148–156. <https://doi.org/10.17605/OSF.IO/59G3V>
- Islam MR, Hayashi D (2008) Geology and coal bed methane resource potential of the Gondwana Barapukuria coal basin, Dinajpur, Bangladesh. *Int J Coal Geol* 75(3):127–143. <https://doi.org/10.1016/j.coal.2008.05.008>
- Kannaujiya S, Chattoraj SL, Jayalath D et al (2019) Integration of satellite remote sensing and geophysical techniques (electrical resistivity tomography and ground penetrating radar) for landslide characterization at Kunjethi (Kalimath), Garhwal Himalaya. *India Natural Hazards* 97(3):1191–1208. <https://doi.org/10.1007/s11069-019-03695-0>
- Kaul H, Sopan I (2012) Land use land cover classification and change detection using high resolution temporal satellite data. *J Environ* 01(04):146–152
- Khalil MI (2020) Coastal groundwater aquifer characterization from geoelectrical measurements- a case study at Kalapara, Patuakhali, Bangladesh. *J Appl Geol.* 5(1):1. <https://doi.org/10.22146/jag.55009>
- Lu D, Mausel P, Brondízio E, Moran E (2004) Change detection techniques. *Int J Remote Sens* 25(12):2365–2401. <https://doi.org/10.1080/0143116031000139863>
- Martin LRG (1989) Accuracy assessment of Landsat-based visual change detection methods applied to the rural-urban fringe. *Photogramm Eng Remote Sens* 55(2):209–215
- Muhammad SB, Abubakar S, Abir IA, Mohammed A (2020) Land subsidence studies of Seberang Perai Malaysia, by integrating remote sensing technique and resistivity survey method. *IOSR J Appl Geol Geophys* 8(1):41–47. <https://doi.org/10.9790/0990-0801034147>
- Oliver-Cabrera T, Wdowinski S, Kruse S, Robinson T (2020) InSAR detection of localized subsidence induced by sinkhole activity in suburban west-central Florida. *Proc Int Assoc Hydrol Sci* 382:155–159. <https://doi.org/10.5194/piahs-382-155-2020>
- Pacheco-Martínez J, Cabral-Cano E, Wdowinski S et al (2015) Application of InSAR and gravimetry for land subsidence hazard Zoning in Aguascalientes, Mexico. *Remote Sens* 7(12):17035–17050. <https://doi.org/10.3390/rs7121586>
- Patra SK, Shekher M, Solanki SS et al (2006) A technique for generating natural colour images from false colour composite images. *Int J Remote Sens* 27(14):2977–2989. <https://doi.org/10.1080/01431160600554322>

- Rahman MM, Woobaidullah ASM (2020) Groundwater resources exploration in a Hillock valley at Lada refugee camp Teknaf using electrical resistivity soundings. *Arab J Geosci.* <https://doi.org/10.1007/s12517-020-5056-y>
- Rawat JS, Kumar M (2015) Monitoring land use/cover change using remote sensing and GIS techniques: a case study of Hawalbagh block, district Almora, Uttarakhand, India. *Egypt J Remote Sens Space Sci* 18(1):77–84. <https://doi.org/10.1016/j.ejrs.2015.02.002>
- Sidhu N, Pebesma E, Câmara G (2018) Using google earth engine to detect land cover change: Singapore as a use case. *Eur J Remote Sens.* 51(1):486–500. <https://doi.org/10.1080/22797254.2018.1451782>
- Singh PK, Kumar S, Singh UC (2011) Evaluation de la ressource en eaux souterraines dans la zone de Gwalior, Inde, au moyen de données satellitaires: Une approche géomorphologique et géophysique intégrée. *Hydrogeol J* 19(7):1421–1429. <https://doi.org/10.1007/s10040-011-0758-6>
- Sunny S (2018) Barapukuria: are people really as content as the government would have us believe? *The Daily Star.* <https://www.thedailystar.net/star-weekend/environment/barapukuria-1587976>. Accessed 10 July 2020
- Thabit JM, Al-zubedi AS (2015) Aquifers delineation using vertical electrical sounding in south and southwest of Samawa city, Southern Iraq. *Iraqi Bull Geol Min* 11(1):133–141
- Tiwari MK, Saxena A (2011) Change detection of land use/landcover pattern in an around mandideep and obedullaganj area, using remote sensing and GIS. *Int J Technol Eng Syst.* 2(3):342–350
- Ulfah S, Marzuki M, Susilo A (2021) Analysis vulnerability disaster of landslide in Lantan village using geoelectric data and sentinel image. *J Penelit Pendidik IPA.* 7(4):794–801. <https://doi.org/10.29303/jppipa.v7i4.915>
- Wenner F (1916) A method of measuring earth resistivity. *Bull Bur Stand* 12(4):469. <https://doi.org/10.6028/bulletin.282>
- Widada S, Saputra S, Hariadi, (2018) Determination of soft lithology causes the land subsidence in coastal Semarang city by resistivity methods. *IOP Conf Ser Earth Environ Sci.* <https://doi.org/10.1088/1755-1315/116/1/012092>
- Widada S, Zainuri M, Yulianto G, Saputra S, Rochaddi B (2019) Distribution of depth and clay-silt to sand ratio of land subsidence in coastal Semarang city by resistivity methods. *J Kel Trop.* 22(1):63. <https://doi.org/10.14710/jkt.v22i1.4463>
- Widada S, Zainuri M, Yulianto G, Satriadi A, Wijaya YJ (2020) Estimation of land subsidence using sentinel image analysis and its relation to subsurface lithology based on resistivity data in the coastal area of Semarang city Indonesia. *J Ecol Eng.* 21(8):47–56. <https://doi.org/10.12911/22998993/127394>
- Woobaidullah A, Rahman MM, Uddin MZ (2016) Evaluation of hydrogeological conditions through vertical electrical soundings survey at Mankiganj pourashava, Manikganj, central part of Bangladesh. *Bangladesh J Sci Res* 27(2):109–120. <https://doi.org/10.3329/bjsr.v27i2.26229>
- Woobaidullah ASM, Islam MA, Hossain MZ, Islam MS (2020) Geo-electrical resistivity survey for fresh groundwater investigation in Mirsharai economic zone, Chittagong in the south-eastern coastal areas of Bangladesh. *J Nepal Geol Soc* 60:181–194. <https://doi.org/10.3126/jngs.v60i.31262>
- Xiong J, Thenkabail PS, Tilton JC et al (2017) Nominal 30-m cropland extent map of continental Africa by integrating pixel-based and object-based algorithms using Sentinel-2 and Landsat-8 data on google earth engine. *Remote Sens.* <https://doi.org/10.3390/RS9101065>
- Xu H, Chen Y (2012) A technique for simulating pseudo natural color images based on spectral similarity scales. *IEEE Geosci Remote Sens Lett* 9(1):70–74. <https://doi.org/10.1109/LGRS.2011.2160710>
- Yan W, Chen J, Tan Y et al (2021) Theoretical analysis of mining induced overburden subsidence boundary with the horizontal coal seam mining. *Adv Civil Eng* 2021:1–7. <https://doi.org/10.1155/2021/6657738>
- Zhu Z (2017) Change detection using landsat time series: a review of frequencies, preprocessing, algorithms, and applications. *ISPRS J Photogramm Remote Sens* 130:370–384. <https://doi.org/10.1016/j.isprsjprs.2017.06.013>

Publisher's Note Springer Nature remains neutral with regard to jurisdictional claims in published maps and institutional affiliations.

Springer Nature or its licensor (e.g. a society or other partner) holds exclusive rights to this article under a publishing agreement with the author(s) or other rightsholder(s); author self-archiving of the accepted manuscript version of this article is solely governed by the terms of such publishing agreement and applicable law.